Methodological Framework for Density Estimation: Insights from Muography Laboratory Measurements and Simulations Experiments

Ahmed Eleslambouly
Khalifa University of Science and Technology

Hamid Basiri
The University of Tokyo

Mohammed Ali
Khalifa University of Science and Technology

Matsushima, Jun
The University of Tokyo

他

https://doi.org/10.5109/7323395

出版情報：Proceedings of International Exchange and Innovation Conference on Engineering & Sciences (IEICES). 10, pp.1100-1106, 2024-10-17. International Exchange and Innovation Conference on Engineering & Sciences
バージョン：

Methodological Framework for Density Estimation: Insights from Muography Laboratory Measurements and Simulations Experiments

Ahmed Eleslambouly[1], Hamid Basiri[2], Mohammed Ali[1], Jun Matsushima[2], Masashi Kodama[3], Toshiyuki Yokota[3], Fateh Bouchalaa[1]
[1] Khalifa University of Science and Technology, [2] The University of Tokyo, [3] Geological Survey of Japan, AIST.
Corresponding author email: Basiri.hamid@edu.k.u-tokyo.ac.jp

Abstract: *Muography is a passive geophysical method that is advancing for multiple imaging applications. In this study, we present a methodological framework for muography to estimate density at a varying density-length. We utilized the muon absorption method to estimate material density, employing both experimental setups with plastic scintillator detectors, acrylic objects and simulations using the PHITS Monte Carlo code. By analyzing muon flux after passing through target materials, we compute an empirical model for density estimation. The findings demonstrate the technique's effectiveness in identifying density variations, with potential applications in geophysical exploration and geological studies. This research aims to advance the precision and reliability of muon-based density estimation by validating the density estimation using simulation and experimental approaches.*

Keywords: Muography; Density estimation; Cosmic Rays; Subsurface imaging.

1. INTRODUCTION

Muons are subatomic particles that share some similarities with electrons, such as having an electric charge, and possessing a spin of ½ intrinsic angular momentum. However, muons differ significantly in terms of mass, as they have a much larger mass of approximately 105.7 MeV/c², which makes them about 207 times heavier than electrons [1]. Due to their large mass, muons are less readily accelerated when they come into contact with electromagnetic fields compared to electrons [2, 3]. High-energy muons originate from galactic cosmic rays (GCRs), which result from the acceleration of particles by supernovas and their remnants within our Milky Way galaxy [4]. Cosmic-ray muons have an energy range of 10 MeV – 100 GeV with an average of 2-4 GeV [3]. The Earth is continually bombarded by cosmic-ray with an approximate flux of 1 muon per square centimeter per minute. The high energy of muon enables them to penetrate deeply into materials such as hundreds of meters and this makes them suitable for geological and underground studies [5-7].

Cosmic-ray muons typically show a higher flux at angles closer to the vertical, decreasing with increasing zenith angles. The azimuth distribution is almost isotropic and can vary based on local geomagnetic conditions and atmospheric effects [8]. As the muons pass through the objects, they have some interactions such as ionization, resulting in muon attenuation due to energy loss or changing direction because of scattering. By analyzing the behavior of muons in the matter, the density of the material can be estimated, and muon imaging becomes feasible.

Following the discovery of cosmic-rays [9-13] and muons [14], muon radiography, currently known as "muography" was introduced by Alvarez, et al. [15]. Since then muography has been utilized for diverse applications including security screening [16, 17], magnetic field imaging [18], nuclear waste monitoring [19], and imaging of damaged core of the Fukushima-Daiichi nuclear power plant [20]. Besides these applications, there was a growing interest in utilizing muon imaging for Earth sciences applications as the cosmic-ray muons provide a passive method for continuous monitoring of subsurface imaging. The initial investigations pertaining to muon imaging were prompted by the necessity to assess the geological material covering underground laboratories that housed particle detectors [9]. Moreover, in recent years, high-energy cosmic-ray muography has been utilized to capture images of the internal structures of geological formations, Tanaka, et al. [21] have developed a real-time volcano monitoring system using muography to monitor the lava flow and mass change detection inside the Asama volcano in Japan. In their work, they have successfully mapped the crater floor density variation after volcanic ash eruption. Morishima, et al. [22] have applied cosmic-ray muon radiography to detect any undiscovered chambers or voids within the pyramid. Matsushima, et al. [23] demonstrated the relationship between the total number of muons counts when the water level in a tank was changing at a fixed time.

Density estimation plays a crucial role in geophysical investigations, providing essential information about subsurface structures and material properties distribution. Accurate density models are vital for various applications, including mineral exploration, geological reservoir characterization, and environmental studies. Geophysical methods, such as seismic and gravity, have been widely employed to estimate subsurface densities. However, despite their extensive use and significant advancements, these methods face several limitations that affect the accuracy and spatial resolution of density estimations [24-27]. Therefore, there is a continuous need to fill this ambiguity. Moreover, muography leaves a passive source nature, making it a cheap method to deploy at various scales and applications for near or deep surface targets.

In our study, we investigate the potential of using muon counts as a primary method for estimating material density. We employ both laboratory measurements and simulation modeling to obtain an empirical model for density estimation based on density length and muon counts. This work emphasizes the critical importance of accurate density estimation in subsurface imaging,

highlighting its role in directly linking to the medium's density. Our research aims to enhance the precision and reliability of density estimation methodologies. By comparing the results from both methods, we aim to enhance the precision and reliability of density estimation techniques, contributing significantly to geophysical subsurface exploration.

2. METHODS AND MATERIALS

In the current study, we employ a dual approach combining laboratory experiments and simulations to investigate the potential of muon counts as a primary method for estimating material density. The laboratory experiments provide real-world data subjected to environmental and atmospheric variations, while the simulations offer controlled conditions to validate and enhance the accuracy of our findings.

2.1 Muons Absorption Method

Charged particles muons, Interact with electrons in medium primarily through ionization while traveling through it. Their energy loss or deviation in direction (scattering angle) is directly related to the thickness and density of the material they pass through. Scientists have developed two muography techniques based on analyzing either the scattering or absorption of muons in matter [30]. In the present work, we are utilizing muons absorption properties to estimate the density of the materials.

Muon absorption techniques involve measuring the flux of muons after they pass through a target material. By comparing the background (reference) measurement and muon fluxes after placing objects, it is possible to determine the amount of energy lost related to attenuation factor of the material and, consequently, the density of the material [28]. This method is particularly effective for dense materials where the attenuation is significant. Thus, their absorption rate is influenced by this density. By assessing the muon flux rate from various directions, it is possible to determine the density variations of the materials situated between the muon source and the detector.

The intensity of cosmic muons can be expressed through the measured count rate. Let I_0 represent the reference measurement and the count rate of muons detected before placing any object in the region of interest, I represent the count rate after passing through the absorbing medium, μ is the attenuation factor, and x represents the path length through the material. Using these parameters, we can derive the following relationship:

$$I = I_0 e^{-\mu x}, \quad (1)$$

If the count rate and the thickness of the absorber are measured, the absorption coefficient can be calculated from the slope obtained by fitting the data to linear using Equation 2.

$$ln\,(I) = \ln(I_0) - \mu x, \quad (2)$$

This equation can be used to determine the absorption coefficient experimentally. The fitting method employed is the least squares technique [29].

2.2 Laboratory Measurements

The diagram in Figure 1 illustrates the laboratory configuration for a muon coincidence measurements with four detectors (CH1, CH2, CH3, CH4). The discriminator outputs are sent to a coincidence detection circuit, which identifies simultaneous events across all detectors, removing unwanted events. When a coincidence is detected, a gate signal is generated to control the multi-channel analyzer, which processes and records the detected events. This setup ensures accurate muon detection by recording only events that trigger all four detectors simultaneously. Figure 2 illustrates the configuration of our laboratory experiment. In this setup, the target object is positioned centrally between four scintillators with dimensions of 20 × 20 cm, which are vertically aligned at the same point. This arrangement is designed to capture coinciding muon events with orientations ranging from vertical to slightly deviated angles. By doing so, we ensure that only muon events passing through the target object are recorded, thereby eliminating any undesired events. Additionally, we added a lead plate of a thickness of 3 cm to eliminate undesired particles such as electrons. An event is recorded when all scintillators react within a threshold window. In our experiment work, we use homogenous acrylic boxes with dimensions of 20 × 20 cm and a density of approximately 1.19 g/cm^3. The experiment initially records the background measurements (events count) for 48 hours per run. Moreover, an acrylic box is added every run until a total of four boxes are in place. This sequence of measurements is performed consecutively and repeated three times to ensure the repeatability and reliability of the data. Additionally, in our present work, we ignore the effect of oblique muon paths, as we assume a very minor effect due to the laboratory configuration and only small deviation in the muon path is expected.

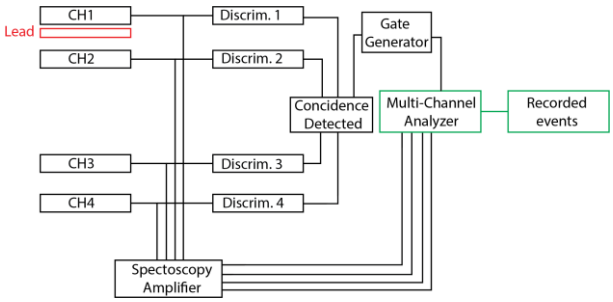

Fig. 1. Diagram illustrating muon coincidence detection setup to record simultaneous events.

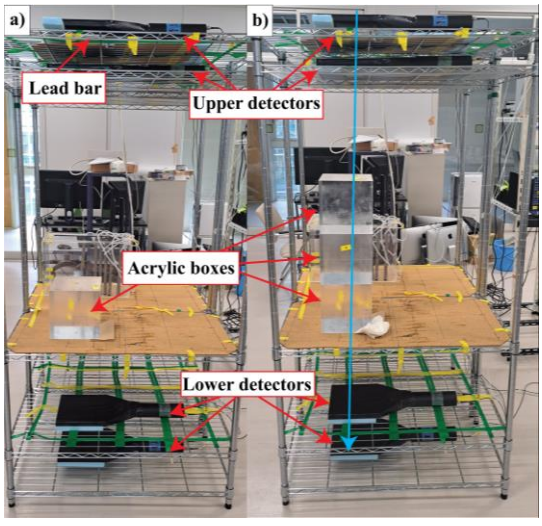

Fig. 2. Image of laboratory measurement using a) one acrylic and b) three acrylic boxes. The blue arrow illustrates a typical recorded coinciding event.

2.3 Data Filtering and Environmental Corrections

The recorded raw data from the multichannel analyzer (MCA) are subjected to bandpass filtering based on the observed muon pulse peak, and removing the random coincidence recorded noise. Furthermore, the muon-recorded counts are subject to environmental corrections [30], to remove the barometric and temperature fluctuations effects and adjust it to the base level. The Barometric effect is explained by the following equation:

$$\left(\frac{\delta I}{I}\right)_P = \beta \,.\, \delta P \,, \qquad (3)$$

Where $\frac{\delta I}{I}$ is the normalized variation of muon flux intensity, β is the barometric coefficient, δP is the pressure variation, calculated as $\delta P = P - P_B$, where P is the current atmospheric pressure and P_B is the base pressure value [31]. Now the temperature effect is given as follows:

$$\left(\frac{\delta I}{I}\right)_T = \int_{h0}^{0} \propto (h) \cdot \delta T(h)\, dh \,, \qquad (4)$$

Where $\propto (h)$ is the temperature coefficient density at height h and $\delta T(h)$ is the temperature variations at height h, calculated as $\delta T = T - T_B$, where T is the temperature during measurement time, and T_B is the base temperature value [32]. In the last step as muon flux is not consistent during the measurement time, we apply an additional filter based on standard deviation (STD), removing data not corresponding to 85% of the measured data counts.

2.4 Simulation Measurements

This setup is complemented by simulation models replicating the lab conditions, allowing for comprehensive analysis and validation of the empirical density estimation model. The simulation modeling components and configuration are shown in Figure 3 where similar geometries are used with reference from the floor to the concrete roof.

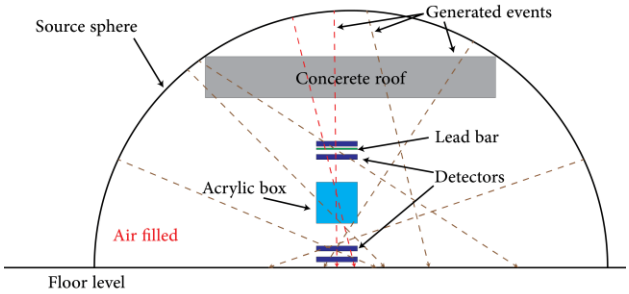

Fig. 3. Schematic illustration of the simulation model used to replicate the lab conditions. The red and brown arrows represent events of interest (coinciding) and no interest, respectively.

We simulate an equivalent event of 24 hours, assuming the following:

$$Total\ events\ /min\ = A \times Muon\ Flux\ (1\frac{muon}{cm^2.min})$$

Where A is the area of the spherical source used, and *Muon flux* is a single event for each square centimeter [33]. In our simulations, we utilize PHITS (Particle and Heavy-Ion Transport code System) Monte Carlo code [34] to simulate muon interactions with our target objects. We use a mono-energy surface source of positive and negative muons and energy ranging from $1e^{-4}$ to 10 GeV (Fig. 3). Cosmic-ray muons are generated based on the PARMA model, which provides a detailed description of the secondary cosmic-ray muon spectrum and its interactions with the Earth's atmosphere [34, 35]. Additionally, the PARMA model helps in accurately replicating the energy spectrum and angular distribution of cosmic-ray muons at different altitudes and depths, ensuring that our simulations closely mirror real-world conditions [36]. This approach provides a robust and reliable simulation environment for studying muon behavior and replicating the experiment environment.

3. RESULTS

In this section, we present a detailed analysis of the results obtained from both laboratory measurements and simulation experiments. The laboratory measurements are subject to uncertainties due to environmental and atmospheric conditions, which can affect the muon flux. These results are then compared with those from the simulation experiments to evaluate the accuracy and reliability of the simulation model in predicting muon flux behavior under controlled conditions.

3.1 Laboratory Measurements

The raw measurement counts, depicting the muon flux as a function of density length, are presented in Figure 4.a. This data is in the range of 300 counts originally, a bandpass filter was applied to remove unwanted events and restrict the data to the muon pulse peak exclusively. The total counts per each stage were reduced in the range of average counts 200 events per hour (Fig. 4.b), where almost a third of acquired data is believed to be of other particle undesired events such as electrons, gamma, and therefore has been filtered. This step is crucial before carrying out any further analysis, as it also showed enhancement in the data fitting to the regression lines.

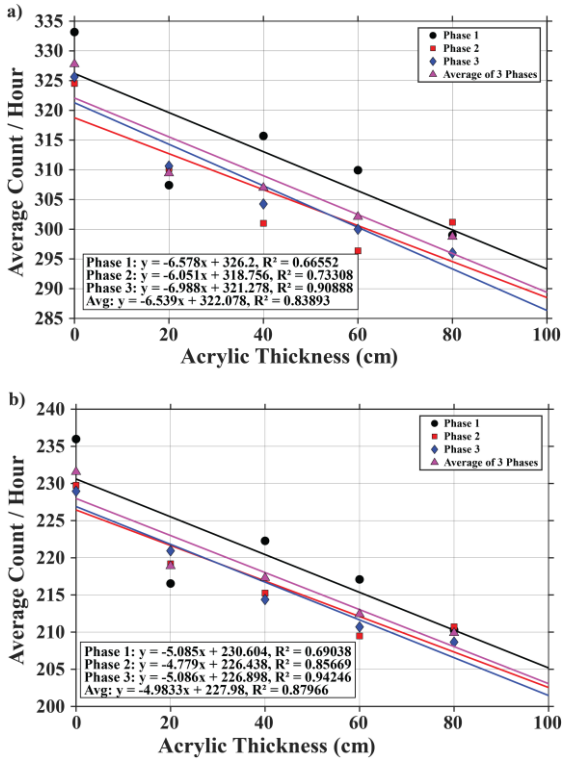

Fig. 4. A scatter plot shows the muon average counts per hour collected from each acquisition phase. a) Raw acquired data, b) after muon peak pulse filtering.

The obtained data from previous steps were subjected to corrections for environmental variations, as demonstrated in Figure 5. Public data on atmospheric temperature and pressure have been collected from Shimoufusa Ab station, Nagayama through Meteostat database [37].This has set all measurements to base conditions and minimized the uncertainty in the counts measurements due to atmospheric conditions variations. The obtained muon counts after environmental corrections show a further enhancement in the fitting to the regression models. In the last step, we apply the final STD filter where the total counts show a high fit to the regression model but vary from stage to stage (Fig. 6.b); a general trend of reduction in the muon counts is noticed between each phase experiment and assumed to be related to seasonal muon flux. The average counts consistently enhanced in fitting the regression model, improving the object material's absorption relationship and density length.

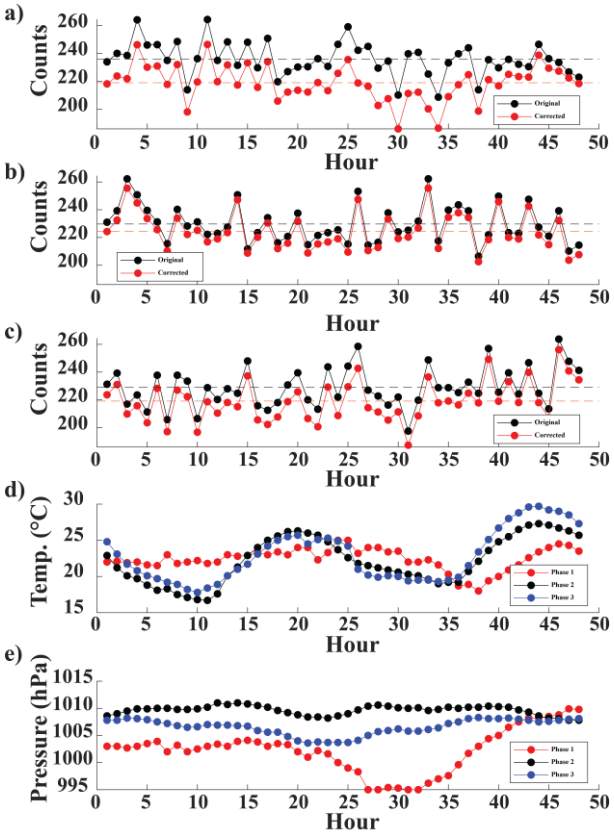

Fig. 5. Diagram illustrating the experimental data collected from background (no acrylic) measurements before and after applying environmental corrections for each measurement phase. Part (a) shows the raw and corrected data for Phase 1, part (b) for Phase 2, and part (c) for Phase 3. Additionally, part (d) presents the temperature records corresponding to each phase of measurements, while part (e) displays the atmospheric pressure records corresponding to each phase.

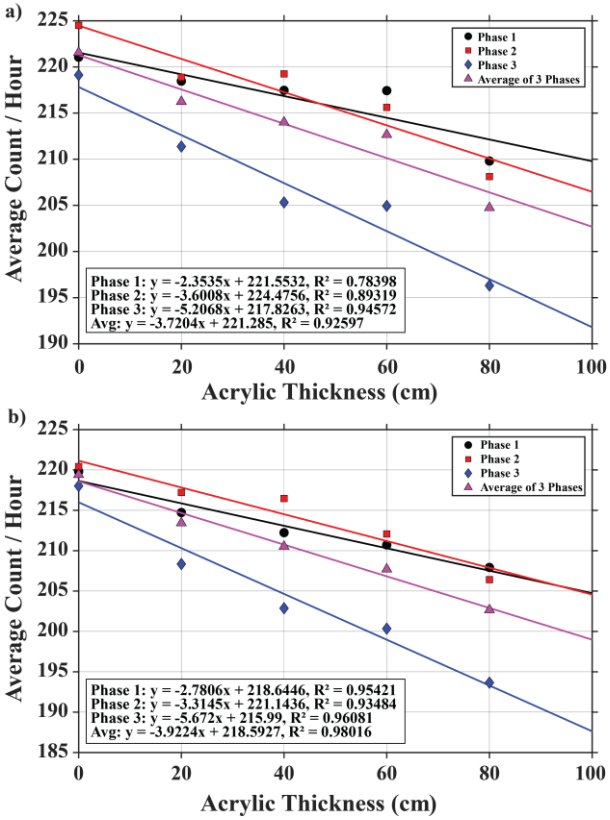

Fig. 6. A scatter plot shows the muon average counts per hour obtained. a) after obtaining muon counts at base-level environmental corrections, b) after the STD filter was applied to the data shown in Figure a.

We apply an exercise to estimate the density using the obtained average muon counts from all the phases using raw collected data and filtered denoised data shown in Table 1. The obtained densities from raw data have a high error at a very short density length compared to other longer density lengths. Meanwhile, the filtered data showed overall better density estimates at various density lengths.

Table 1. Density estimations using laboratory experiment data

	Acrylic cubes	Density length (g/cm2)	Estimated density (g/cm3)	Relative error (%)
Raw Data	1	38.74	1.937	62.76
	2	46.18	1.154	2.99
	3	61.11	1.019	14.41
	4	71.39	0.892	25.01
Filtered Data	1	26.34	1.317	10.65
	2	51.15	1.029	13.56
	3	55.48	0.925	22.29
	4	81.23	1.015	14.67

3.2 Simulation Measurements

The simulation results, depicting the muon flux as a function of density length, are presented in Figure 7. We use measurement counts from each stage to estimate the attenuation coefficient and determine the slope to best regression fit. The estimated densities from density length computation are as follows in Table 2.

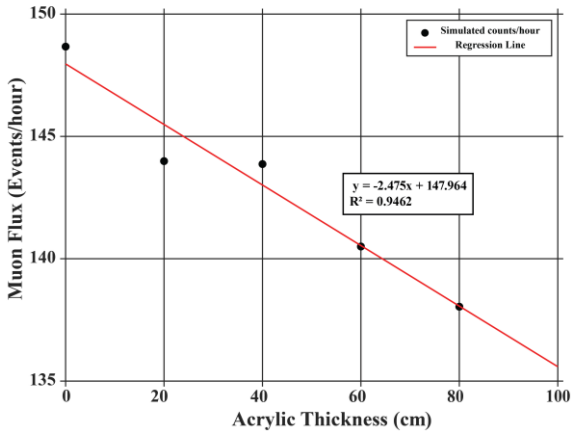

Fig. 7. Scatter plot showing obtained muon flux from simulations for each acrylic experiment fitted to regression model.

Table 2. Density estimations using simulation experiment data.

Acrylic cubes	Density length (g/cm2)	Estimated density (g/cm3)	Relative error (%)
1	32.11	1.606	34.93
2	33.08	0.827	30.50
3	60.32	1.005	15.52
4	80.19	1.002	15.76

The density estimations at shorter density lengths exhibit higher relative errors than those at longer density lengths, which are more accurate. Specifically, the relative errors for the shortest density lengths (32.11 g/cm² and 33.08 g/cm²) are significantly higher (34.93% and 30.50%, respectively) compared to those for longer density lengths (60.32 g/cm² and 80.19 g/cm²), which are 15.52% and 15.76%, respectively. This indicates that as the density length increases, the accuracy of the estimated density improves. Therefore, the computed relative error in density decreases as the density length increases, indicating a clear relationship between the accuracy of density length and its fitting to the regression model. This correlates to the same behavior observed in the raw data and single stages trendline.

4. DISCUSSION

The study presented here demonstrates the effectiveness of muography as a method for density estimation through a combination of laboratory measurements and simulation experiments. The results obtained from raw (Fig. 4.a) and filtered data (Fig. 6.b) highlight the critical role of data processing in improving the accuracy and reliability of density estimations. Overall, a higher error is observed for density estimations at smaller density lengths as shown in Tables 1 & 2, attributed to various factors, including the sensitivity of the measurements at such a small scale, environmental noises, experimental setup limitations, and inherent fluctuations in muon flux. A better density estimate is obtained at longer density lengths in both raw and filtered datasets. Further measurement at higher density lengths can increase the accuracy of density estimations and can lead to more accurate density.

The simulation results were consistent with the laboratory measurements, reinforcing the validity of our methodological framework. However, the relative errors in the simulation data were generally lower than those observed in the raw experimental data due to the contribution of other particle events; however, still exhibited similar trends. This discrepancy is primarily due to the controlled conditions in simulations, which eliminate many of the environmental variables affecting real-world measurements. Nonetheless, the simulations provided valuable insights into the behavior of muon flux through different density lengths, corroborating the empirical findings and validating the data obtained from laboratory experiments.

The ability to accurately estimate density using muography has significant implications for geophysical exploration and geological studies. The method's precision in identifying density variations makes it a valuable tool for subsurface imaging, mineral exploration, and environmental studies. By enhancing the accuracy and reliability of density estimations, muography can contribute to more detailed and comprehensive geological models, aiding in the identification of subsurface structures and material properties. This research advances the precision and reliability of muon-based density estimation by validating the density estimation using both simulation and experimental approaches.

5. CONCLUSIONS

This study demonstrates the effectiveness of muography for density estimation through both laboratory measurements and simulations. We found that data filtering and environmental corrections significantly improve accuracy, with filtered data showing lower relative errors than raw data. Longer density lengths provide more reliable estimations due to better regression model fitting, while shorter lengths have higher deviations and errors. The improved accuracy at higher density lengths is due to a better representation of the material's true attenuation properties, reducing measurement noise and uncertainties.

Our results, consistent between simulations and laboratory measurements, validate our methodological framework and enhance confidence in using muography for density estimation. Accurate density estimation through muography has significant implications for geophysical exploration and geological studies, improving subsurface imaging and monitoring, mineral exploration, and environmental studies. This research advances the precision and reliability of muon-based density estimation, contributing to geophysical subsurface exploration.

6. ACKNOWLEDGEMENT

This work was supported by the Mohammed bin Salman Center for Future Science and Technology for Saudi Arabia-Japan Vision 2030 at the University of Tokyo (MbSC2030).

7. REFERENCES

[1] I. R. Kenyon, Elementary particle physics. Springer Science & Business Media, 1987.

[2] H. K. Tanaka, "Subsurface density mapping of the earth with cosmic ray muons," Nuclear Physics B-Proceedings Supplements, vol. 243, pp. 239-248, 2013.

[3] H. Basiri, T. Kin, and N. Okamoto, "The influence of magnetic field on muography images: A simulation study," 2021.
[4] E. Parizot, "Cosmic ray origin: lessons from ultra-high-energy cosmic rays and the Galactic/extragalactic transition," Nuclear Physics B-Proceedings Supplements, vol. 256, pp. 197-212, 2014.
[5] A. Lechmann et al., "Muon tomography in geoscientific research–a guide to best practice," Earth-science reviews, vol. 222, p. 103842, 2021.
[6] G. Bonomi, P. Checchia, M. D'Errico, D. Pagano, and G. Saracino, "Applications of cosmic-ray muons," Progress in Particle and Nuclear Physics, vol. 112, p. 103768, 2020.
[7] M. Holma, Z. Zhang, P. Kuusiniemi, K. Loo, and T. Enqvist, "Future prospects of muography for geological research and geotechnical and mining engineering," Muography: Exploring Earth's Subsurface with Elementary Particles, pp. 199-219, 2022.
[8] J. S. George et al., "Elemental Composition and Energy Spectra of Galantic Cosmic Rays During Solar Cycle 23," The Astrophysical Journal, vol. 698, no. 2, p. 1666, 2009/06/03 2009.
[9] E. George, "Cosmic rays measure overburden of tunnel," Commonwealth Engineer, vol. 455, 1955.
[10] P. Auger, "Les rayons cosmiques," presented at the PUF, Paris, 1941.
[11] L. Leprince-Ringuet, "Les rayons cosmiques," presented at the Albin Michel,, Paris, 1948.
[12] T. Gaisser, "Cosmic rays and particle physics, Cambridge, UK: Univ," ed: Pr, 1990.
[13] M. Crozon, "Quand le ciel nous bombarde," presented at the Vuibert, Paris, 2005.
[14] S. H. Neddermeyer and C. D. Anderson, "Cosmic-ray particles of intermediate mass," Physical Review, vol. 54, no. 1, p. 88, 1938.
[15] L. W. Alvarez et al., "Search for Hidden Chambers in the Pyramids: The structure of the Second Pyramid of Giza is determined by cosmic-ray absorption," Science, vol. 167, no. 3919, pp. 832-839, 1970.
[16] K. Borozdin et al., "Cosmic-ray muon tomography and its application to the detection of high-z materials," in Proceedings of the 46th Annual Meeting, Institute of Nuclear Materials Management, 2005: Citeseer, pp. 1-8.
[17] W. C. Priedhorsky et al., "Detection of high-Z objects using multiple scattering of cosmic ray muons," Review of Scientific Instruments, vol. 74, no. 10, pp. 4294-4297, 2003.
[18] H. Basiri, T. Kin, N. Okamoto, A. Giammanco, and E. C. Gil, "Simulation of a First Case Study for Magnetic Field Imaging with the Magic-μ Technique," Journal of Advanced Instrumentation in Science, 2022.
[19] G. Jonkmans, V. Anghel, C. Jewett, and M. Thompson, "Nuclear waste imaging and spent fuel verification by muon tomography," Annals of Nuclear Energy, vol. 53, pp. 267-273, 2013.
[20] H. Miyadera et al., "Imaging Fukushima Daiichi reactors with muons," Aip Advances, vol. 3, no. 5, 2013.
[21] H. K. Tanaka, T. Uchida, M. Tanaka, H. Shinohara, and H. Taira, "Cosmic-ray muon imaging of magma in a conduit: Degassing process of Satsuma-Iwojima Volcano, Japan," Geophysical Research Letters, vol. 36, no. 1, 2009.
[22] K. Morishima et al., "Discovery of a big void in Khufu's Pyramid by observation of cosmic-ray muons," Nature, vol. 552, no. 7685, pp. 386-390, 2017.
[23] J. Matsushima et al., "Combined measurement of cosmic ray muons and elastic waves on a laboratory scale : a follow-up report," Proceedings of the SEGJ Conference, vol. 148, pp. 113-115, 2023 2023.
[24] O. Eiken, M. Zumberge, and G. Sasagawa, "Gravity monitoring of offshore gas reservoirs," in SEG Technical Program Expanded Abstracts 2000: Society of Exploration Geophysicists, 2000, pp. 431-434.
[25] M. Zumberge, H. Alnes, O. Eiken, G. Sasagawa, and T. Stenvold, "Precision of seafloor gravity and pressure measurements for reservoir monitoring," Geophysics, vol. 73, no. 6, pp. WA133-WA141, 2008.
[26] V. Kolesov and K. Gareev, "Application of Time Lapse Gravity Measurements for Oil and Gas Field Development Monitoring," in SPE Russian Petroleum Technology Conference, 2019: OnePetro.
[27] C. Jenkins, A. Chadwick, and S. D. Hovorka, "The state of the art in monitoring and verification—ten years on," International Journal of Greenhouse Gas Control, vol. 40, pp. 312-349, 2015.
[28] S. Procureur, "Muon imaging: Principles, technologies and applications," Nuclear Instruments and Methods in Physics Research Section A: Accelerators, Spectrometers, Detectors and Associated Equipment, vol. 878, pp. 169-179, 2018.
[29] R. N. Altameemi, N. S. A. Hamid, W. M. A. W. M. Kamil, and S. M. S. Ahmed, "Determination of muon absorption coefficients in heavy metal elements," Journal of Radiation Research and Applied Sciences, vol. 12, no. 1, pp. 281-288, 2019.
[30] M. Berkova, V. Grigoryev, M. Preobrazhensky, A. Zverev, and V. Yanke, "Temperature effect observed for the muon component in the yakutsk cosmic-ray spectrograph," Physics of Atomic Nuclei, vol. 81, pp. 776-785, 2018.
[31] R. De Mendonca, J. P. Raulin, E. Echer, V. Makhmutov, and G. Fernandez, "Analysis of atmospheric pressure and temperature effects on cosmic ray measurements," Journal of Geophysical Research: Space Physics, vol. 118, no. 4, pp. 1403-1409, 2013.
[32] M. Berkova, A. Belov, E. Eroshenko, and V. Yanke, "Temperature effect of muon component and practical questions of how to take into account in real time," Astrophysics and Space Sciences Transactions, vol. 8, no. 1, pp. 41-44, 2012.
[33] K. A. Olive, "Review of particle physics," Chinese physics C, vol. 38, no. 9, p. 090001, 2014.
[34] T. Sato et al., "Features of particle and heavy ion transport code system (PHITS) version 3.02," Journal of Nuclear Science and Technology, vol. 55, no. 6, pp. 684-690, 2018.

[35] T. Sato, H. Yasuda, K. Niita, A. Endo, and L. Sihver, "Development of PARMA: PHITS-based analytical radiation model in the atmosphere," Radiation research, vol. 170, no. 2, pp. 244-259, 2008.
[36] T. Sato, "Analytical model for estimating the zenith angle dependence of terrestrial cosmic ray fluxes," PloS one, vol. 11, no. 8, p. e0160390, 2016.
[37] MeteoStat. Atomspheric Climate Data [Online] Available: https://meteostat.net/en/place/jp/nagareyama